

Hydra: A mixture modeling framework for subtyping pediatric cancer cohorts using multimodal gene expression signatures

Jacob Pfeil^{1,2*}, Lauren M. Sanders^{1,2,3}, Ioannis Anastopoulos^{1,2}, A. Geoffrey Lyle^{2,3}, Alana S. Weinstein^{1,2}, Yuanqing Xue^{1,2}, Andrew Blair^{1,2}, Holly C. Beale^{2,3}, Alex Lee⁴, Stanley G. Leung⁴, Phuong T. Dinh⁴, Avanthi Tayi Shah⁴, Marcus R. Breese⁴, W. Patrick Devine⁵, Isabel Bjork², Sofie R. Salama^{1,2,6†}, E. Alejandro Sweet-Cordero^{4†}, David Haussler^{1,2,6†}, Olena Morozova Vaske^{2,3†}

1 Department of Biomolecular Engineering, University of California, Santa Cruz, California, United States of America

2 Genomics Institute, University of California, Santa Cruz, California, United States of America

3 Department of Molecular, Cell and Developmental Biology, University of California, Santa Cruz, California, United States of America

4 Department of Pediatrics, Division of Hematology and Oncology, University of California, San Francisco, California, United States of America

5 Department of Anatomic Pathology, University of California, San Francisco, California, United States of America

6 Howard Hughes Medical Institute, University of California, Santa Cruz, California, United States of America

†Senior authorship

* Corresponding author: jpfeil@ucsc.edu

Abstract

Precision oncology has primarily relied on coding mutations as biomarkers of response to therapies. Incorporation of transcriptome analysis into precision oncology workflows has presented numerous challenges. For example, the relative rather than absolute gene expression level needs to be considered, requiring differential expression analysis across samples. However, expression programs related to the cell-of-origin and tumor microenvironment effects confound the search for cancer-specific expression changes. To address these challenges, we developed an unsupervised clustering approach for discovering differential pathway expression within cancer cohorts using gene expression measurements. The hydra approach uses a Dirichlet process mixture model to automatically detect multimodally distributed genes and expression signatures. We demonstrate that the hydra approach is more sensitive than widely-used gene set enrichment approaches for detecting multimodal expression signatures. Application of the hydra analysis framework to small blue round cell tumors (including rhabdomyosarcoma, synovial sarcoma, neuroblastoma, Ewing sarcoma, and osteosarcoma) identified expression signatures associated with changes in the tumor microenvironment. The hydra approach also identified an association between ATRX deletions and elevated immune marker expression in high-risk neuroblastoma. Notably, hydra analysis of all small blue round cell tumors revealed similar subtypes, characterized by changes infiltrating immune and fibroblast expression signatures.

Author summary

Pediatric cancers generally have few somatic mutations. To increase the number of actionable treatment leads, precision pediatric oncology initiatives also analyze tumor gene expression patterns. However, currently available approaches for gene expression data analysis in the clinical setting often use arbitrary thresholds for assessing over-expression and assume gene expression is normally distributed. These methods also rely on background distributions for assessing expression distributions which over-estimate the uncertainty in the analysis. We developed a computational framework to automatically detect multimodal expression distributions within well-defined disease populations. Our analysis of small blue round cell tumors (including rhabdomyosarcoma, synovial sarcoma, neuroblastoma, Ewing sarcoma and osteosarcoma) discovered a significant number of multimodally expressed genes. Multimodally expressed genes were associated with proliferative signaling, extracellular matrix organization, and immune signaling pathways across cancer types. Expression signatures correlated with differences in patient outcomes for MYCN non-amplified neuroblastoma, osteosarcoma, and synovial sarcoma. The low mutation rate in pediatric cancers has led some to suggest that pediatric cancers are less immunogenic. However, our analysis suggests that immune infiltration can be identified across small blue round cell tumors. Thus, further research into modulating immune cells for patient benefit may be warranted.

Introduction

Large cancer sequencing projects, including The Cancer Genome Atlas (TCGA) and Therapeutically Applicable Research to Generate Effective Treatments (TARGET), have facilitated the development of cancer gene expression compendia [1–6], but these compendia often lack expression data from corresponding normal tissue. Without the normal comparator, Hoadley et al. (2018) found that cell-of-origin signals drive integrative clustering of TCGA data. Strong cell-of-origin and tumor microenvironment (TME) signals may also complicate the interpretation of gene expression results for precision oncology applications, so careful modeling of the data is necessary to infer accurate conclusions.

The TME includes tumor cells, stromal fibroblasts, immune cells, and vasculature [7]. Similarities in TME composition across tumor samples have led to the identification of TME states (e.g. inflamed, immune-excluded, immune-desert). While these states are dynamic, they can still shed light on the immunogenicity of tumor cells and correlate with response to cancer immunotherapies [8]. The TME cellular composition can be inferred from tumor RNA-Seq data since host cell RNA is sequenced along with the cancer cell RNA. Tumor progression and response to therapies is associated with features of the TME. Therefore, targeting the TME therapeutically may improve treatment outcomes in some cancers.

Immunotherapies that activate the host immune system to eradicate tumors have been effective in treating several cancer types, particularly in cancers with a high mutation burden [9, 10]. Pediatric cancers are thought to be less immunogenic than adult cancers because they generally have a lower mutation burden. In addition to infiltrating immune cells, cancer-associated fibroblasts (CAFs) assist in extracellular matrix remodeling and activation of growth factor signaling. CAFs facilitate tumor growth, metastasis, and resistance to some therapies, so identification of CAF functions within a tumor may also facilitate clinical decision making. Methods are needed to both infer and characterize gene expression subtypes that correlate with tumor microenvironment states to accelerate the development of personalized therapies for pediatric cancers.

Tumor/normal differential expression analysis in which a cohort of tumor tissues is compared to corresponding normal tissue samples is an effective approach for identifying gene expression biomarkers [11–13], but it is often not possible to conduct this analysis in a clinical setting. Sufficient biological and technical replicates are limited by tumor tissue availability, and healthy neighboring tissue often cannot be isolated. In addition, for many pediatric cancers, the cell-of-origin, and thus the appropriate reference normal tissue, is not known. Besides differential expression analysis, single-sample pathway analysis can be used to identify upregulation of biological gene sets in tumor subtypes. Among the most widely used pathway analysis approaches is gene set enrichment analysis (GSEA) [14, 15]. GSEA identifies coordinated expression of pathway genes using gene ranks and a Kolmogorov-Smirnov-like test statistic. GSEA is usually performed on differentially expressed genes to compare two cohorts or phenotypes, but single-sample GSEA is also available when there is not an obvious comparator. GSEA uses curated pathway gene sets like those in the Molecular Signatures Database (MSigDB) [16].

Cancer gene expression subtypes are traditionally identified using unsupervised clustering methods such as consensus clustering analysis [17–19]. These methods are generally underpowered because the number of genes greatly exceeds the number of samples. Dimensionality reduction approaches such as Principal Component Analysis (PCA) have been found to underestimate the dimensionality of gene expression data [20]. Lenz et al. (2016) found two cases in which PCA fails to identify a biological signal: when the size of the cluster is small and when the effect size is small. Lenz et al. (2016) suggest investigating multimodally expressed genes to improve identification of subtypes. Cancer subtypes naturally lead to multimodal expression patterns in which each subtype expresses genes certain genes at distinct levels and with unique correlation patterns. Furthermore, enriching for multimodally expressed genes before clustering has been shown to improve correlations with clinical features of interest [21].

Gaussian mixture models are a powerful class of unsupervised clustering algorithms that can be used to detect multimodally expressed genes [22–24]. A Gaussian mixture model is appropriate when the expression data can be modeled as a mixture of two or more Gaussian distributions [25]. One limitation of Gaussian mixture models in this context is that the number of clusters in the data is often not known beforehand, so a parameter search must be used to identify the best-performing model. However, this is a computationally expensive approach. This problem can be overcome by placing a Dirichlet process prior on the number of expression clusters. The number of clusters is then inferred while fitting the mixture model using Markov chain Monte Carlo sampling [25]. This approach has not been widely used in clinical cancer research because these algorithms are still computationally expensive, but recent advances in Bayesian variational inference has made this approach scalable for precision oncology applications [26].

Here, we develop the hydra framework for identifying clinically relevant expression subtypes and classifying N-of-1 tumor samples using learned models. We provide an overview of the hydra framework, assess performance for detecting differential pathway expression, and apply the framework to better understand expression patterns in high-risk neuroblastoma and other small blue round cell tumors. We apply the learned models trained on publicly available cancer gene expression data to the N-of-1 setting and show that this framework can identify distinct immune and stromal expression signatures that differentiate pediatric cancer samples. Finally, we identify recurrent tumor microenvironment signatures across pediatric cancer types associated with differences in patient outcomes.

Materials and methods

Dirichlet Process Gaussian Mixture Model

Traditional parametric models, like the finite mixture model, use a fixed number of parameters (i.e. number of clusters). Over- or underfitting can occur when the parametric model does not reflect the underlying data [27]. Unlike the finite mixture model, the Dirichlet process mixture model (DPMM) represents a theoretically infinite number of clusters and can adapt the number of clusters based on prior belief and the data [25, 27, 28].

The Dirichlet process (*DP*) is an infinite dimensional extension of the Dirichlet distribution [29] and is commonly used as a prior distribution for infinite mixture models [30, 31]. The Dirichlet process has two parameters: the concentration parameter α and centering distribution H . The concentration parameter α , where $\alpha \in \mathbb{R}^+$, controls the extent to which samples from the *DP* resemble the centering distribution H . We model gene expression as a multivariate Gaussian distribution, so our centering distribution is a normal-Wishart distribution ($\mathcal{N}\mathcal{W}_0$).

We briefly describe the stick-breaking construction of the Dirichlet process $G \sim DP(\alpha, H)$ [25, 27, 29, 32]. Consider a stick of unit length. To generate an infinite number of mixing weights $\pi_1, \pi_2, \dots, \pi_k$ for the DPMM, first break a stick of unit length at $\nu \in [0, 1]$ where ν is sampled from a Beta distribution, and set π_1 to be the length of the first piece. We repeat this process using the remainder of the stick for each π_k . The DP is truncated to the number of clusters K , which was shown to accurately approximate the infinite posterior for large K [32].

$$\nu \sim \text{Beta}(1, \alpha) \quad (1)$$

$$\pi_k = \nu_k \prod_{l=1}^{k-1} (1 - \nu_l) \quad (2)$$

Next, we sample the parameters from the centering distribution H weighted by the mixing components. If we consider a probability space Θ where $\theta_k^* \in \Theta$, then H is a measure on the partitions of Θ . For our application, we will partition the parameter space Θ into finite, measurable partitions B_1, B_2, \dots, B_k .

$$\theta_k^* \sim H \quad (3)$$

$$G = \sum_{k=1}^{\infty} \pi_k \delta_{\theta_k^*} \quad (4)$$

$$(G(B_1), G(B_2), \dots, G(B_k)) \sim \text{Dir}(\alpha H(B_1), \alpha H(B_2), \dots, \alpha H(B_k)) \quad (5)$$

This construction generates the marginal of the Dirichlet process, which follows a Dirichlet distribution. Samples from the marginal distribution are finite, discrete, and sum to 1 [29]. Next, we outline how the DPMM groups gene expression samples x_i under cluster-specific parameters μ_{z_i} and Σ_{z_i} where $z_i \in 1, 2, \dots, K$ is the cluster index.

$$x_i | \mu_{z_i}, \Sigma_{z_i} \sim \mathcal{N}(\mu_{z_i}, \Sigma_{z_i}) \quad (6)$$

$$z_i | \pi \sim \text{Categorical}(\pi_1, \pi_2, \dots, \pi_k) \quad (7)$$

$$\mu_{z_i}, \Sigma_{z_i} | G \sim G \quad (8)$$

$$G | \alpha, \mathcal{N}\mathcal{W}_0 \sim DP(\alpha, \mathcal{N}\mathcal{W}_0) \quad (9)$$

We found that standard Markov Chain Monte Carlo (MCMC) inference algorithms, like the collapsed Gibbs sampler [30, 33], over-estimate the number of clusters. For this reason, we incorporated the bnpy memoized online variational inference algorithm (moVB) [32] into our analysis framework. The moVB algorithm uses variational inference to approximate the posterior distribution and interleaves birth, merge, and delete moves to avoid local optima and remove redundant clusters [34].

Hydra Method

We developed a Bayesian non-parametric clustering framework for identifying biological and technical variation in large cancer gene expression datasets without the need for a reference normal dataset. To our knowledge, this is the first reproducible and widely deployable implementation of a non-parametric mixture model framework designed to overcome the challenges of precision oncology gene expression analysis. The *hydra* pipeline is an open source software tool hosted on GitHub (www.github.com/jpfeil/hydra). A Docker container is available for deployment across environments (<https://hub.docker.com/r/jpfeil/hydra>).

The *hydra* framework contains three main command-line tools: *filter*, *enrich*, and *sweep* (Fig 1). The *filter* command is run first to isolate the multimodally expressed genes using a univariate Dirichlet Process Gaussian Mixture Model (DP-GMM). There are two methods for analyzing the resulting set of multimodally expressed genes. The *enrich* method subsets to the genes found to be significantly enriched in biological pathways, and the *sweep* method, which searches within user-defined gene sets for multimodal expression signatures. The underlying analysis routines can be accessed within the docker using Jupyter notebooks to facilitate the development of user-defined workflows.

The *filter* command takes an expression matrix and filters the genes down to the multimodally expressed genes using the DP-GMM described above. We apply a DP-GMM to each gene, saving the model for genes with two or more expression clusters. This creates a directory of multimodally expressed gene models which can be used to predict differential expression in new samples. This analysis framework is a novel contribution to the precision medicine research community. Our approach has several beneficial properties. For example, training models on curated data sets and applying the models to new samples avoids the use of reference distributions, which over-estimate the uncertainty in the analysis by not accounting for subtype expression. Furthermore, this approach identifies the set of most strongly differentially expressed genes within a disease context, which may enrich for potential biomarkers for precision medicine applications. The directory of multimodally expressed genes are also used in downstream clustering analysis. The *enrich* and *sweep* routines are two independent analyses to explore multimodal expression in pediatric cancer gene expression cohorts. In addition to identifying expression variation within a disease context, we also found that multimodally expressed genes that participate in a biological pathway tend to have correlated expression distributions. This insight facilitates the detection of multimodal expression signatures by enriching for genes that have multimodal expression distributions and participate in known biological processes. The *hydra* software comes prepackaged with popular gene sets, including the Molecular Signatures Database (MSigDB) [16], the Gene Ontology terms [35, 36], and the EnrichmentMap gene sets [37]. The gene set database is configurable, so additional gene sets can be added at runtime.

The *enrich* command uses a hypergeometric test [38] to discover enrichment of multimodally expressed genes within a user-defined database of gene sets. This creates a list of gene sets and a list of enriched gene set genes. The *enrich* method outputs a table of enriched gene sets while also clustering samples across the genes that participate in the enriched gene sets. The table of enriched gene sets may reveal

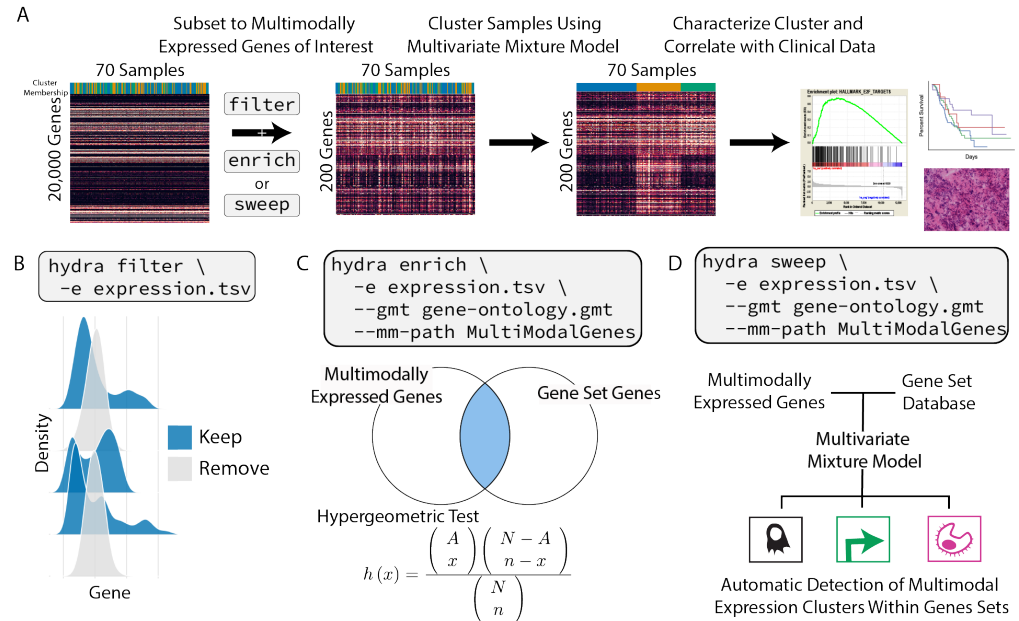


Fig 1. Overview of the hydra framework tools. A: Suggested workflow for applying hydra framework tools to identify clinically relevant gene expression subtypes. B: The hydra *filter* command removes unimodally distributed genes which greatly reduces the number of genes in downstream clustering analysis. C: The hydra *enrich* command takes the multimodally expressed genes and returns enriched gene sets. The enriched gene set genes are used for multivariate clustering of samples. D: The hydra *sweep* command looks for multivariate normal clusters within user-defined gene sets. This can be used for the automatic detection of clusters in large gene set databases.

surprisingly expression patterns and generate hypotheses for further investigation of tumor subtypes. The implementation of the *enrich* method includes an important parameter known as the minimum component probability. The minimum component probability is the probability of placing a sample within the smallest expression cluster. This is an additional filter to remove multimodally expressed genes that influence a relatively small subset of tumor samples. This parameter gives the user the ability to subset the enriched genes to those that influence a greater number of patients. To aid in the exploration of minimum component thresholds, we implemented a *scan* sub-routine. The *scan* routine tunes the analysis with respect to the constraints of the available data (e.g. number of samples and number of genes), which is an important factor in pediatric cancer research since data is often difficult to obtain and so datasets are relatively small. We recommend setting this threshold such that the number of genes is less than the number of samples.

The *sweep* routine identifies differentially expressed gene sets and can be used as an alternative to GSEA [14]. For each gene set, a multivariate DP-GMM is applied to determine if more than one expression cluster is present within the gene set. This approach is useful when curated gene sets are available for the disease of interest, but manual inspection of each gene set is not feasible. Reducing the genes to multimodally expressed genes facilitates the detection of differentially expressed gene sets, since the expression within a subtype is correlated. Existing gene set enrichment tools are known to under-perform when the expression is correlated [39], but our approach is designed to identify distinct correlation structures within gene expression data.

We have also implemented routines for cluster profiling and N-of-1 tumor analysis.

These routines are accessible within the docker container using the Jupyter notebook command. Cluster profiling analysis of clusters derived from the *enrich* or *sweep* routines includes GSEA [40] to identify the pathway expression that characterizes each cluster. GSEA uses all available genes since it requires non-differentially expressed genes to assess the significance of an enrichment score. A t-statistic is calculated for each gene, comparing gene expression values of samples inside to those outside of a cluster. Cluster profiling GSEA uses the ranked gene-level t-statistics to determine gene set enrichment.

The N-of-1 tumor analysis routine classifies a new gene expression profile into one of the inferred clusters, calculates a gene-level z-score for that sample relative to the normalized expression distribution, and performs GSEA. This procedure can identify new gene expression signatures that may not be detectable using the entire expression cohort as a background reference distribution. This approach is another novel contribution to the field and may facilitate the identification of clinically relevant signatures that are being overlooked in current gene expression analyses.

Synthetic Data Generation and Validation

We first tested the hydra framework's ability to detect differential pathway expression using synthetic cancer data. We compared hydra to two widely used gene set enrichment tools: single-sample gene set enrichment analysis (ssGSEA) and gene set variation analysis (GSVA) [41–43]. Both methods are implemented in the GSVA R package [42]. We modeled cancer gene expression as a multivariate Gaussian distribution. We used the TCGA glioblastoma multiforme cohort (N=166) to model a background mean and covariance matrix. This approach allowed us to model cancer gene expression data while also controlling for subtype-related expression variation. We downloaded the RSEM-quantified TPM normalized gene expression measurements from the UCSC Xena Browser [3]. We focus our analysis on normalized gene expression data because this data is more widely used in the cancer research community and fewer methods are available to analyze normalized counts. To reduce heteroscedasticity and the effect of outlier expression levels, we transformed the expression data to $\log_2(\text{TPM} + 1)$ [44].

We defined an expression subtype as a subset of samples with a distinct expression mean and correlation structure compared to other samples within the disease cohort. To avoid biases in the synthetic data generation process, we used random sampling to select MSigDB gene sets for each subtype, the size of the subtype, and the correlation structure within the subtype. We randomly generated a covariance matrix for the cancer subtype expression data, but used the underlying covariance matrix of the TCGA glioblastoma multiforme dataset for the background samples. We tested the effect of having 10% and 25% of genes within a gene set being differentially expressed (%DEG). In addition to these parameters, we tested a range of effect sizes: 0.25 (least different), 0.5, 0.75, 1.0, 1.5, 2.0, 2.5, and 3.0 (most different). This process was repeated twice for each gene set to create synthetic training and test data, which resulted in the generation of 640 synthetic datasets.

We then applied the hydra framework using the hydra *sweep* command (Fig 1). The mean expression filter removed any genes with a mean expression of fewer than 1.0 $\log_2(\text{TPM} + 1)$. This avoids lowly-expressed genes that may have particularly noisy expression measurements. The prior on the hydra covariance matrix was the identity scaled by 2.0 and the prior on the number of clusters was set to 2 because we expect there to be an activated cluster and a baseline expression cluster. We set the over-expressing cluster to be the cluster with the largest L1 norm.

Pediatric Cancer Gene Expression Data

We downloaded pediatric cancer RNA-Seq data for neuroblastoma, osteosarcoma, Ewing sarcoma, alveolar rhabdomyosarcoma, and embryonal rhabdomyosarcoma from the UCSC Treehouse Compendium (<https://treehousegenomics.soe.ucsc.edu/public-data/>). This data was produced using the same RNA-seq pipeline, so potential computational batch effects are minimized [1, 6]. Clinical data for the TARGET neuroblastoma and osteosarcoma samples were obtained from the TARGET Data Matrix (<https://ocg.cancer.gov/programs/target/data-matrix>). We also analyzed a set of 58 synovial sarcoma microarray profiles with matching metastasis rate data [45].

TARGET Neuroblastoma Analysis

The hydra *filter* method included all genes with a mean expression greater than $1.0 \log_2(\text{TPM} + 1)$, a minor expression component probability of at least 20%, and a minimum effect size of 1.0. Our synthetic data analysis found that the signal decreases below an effect size of 1.0, so we use this parameter value for all following analyses. We set a minimum mean threshold of $1.0 \log_2(\text{TPM} + 1)$ to exclude lowly expressed genes that may have unstable measurements. We used the hydra *scan* routine to search a range of minimum component probability thresholds and found 20% yielded the most clusters while keeping the number of genes ($p = 42$) below the number of samples ($n = 70$).

The hydra *enrich* command identified correlated expression signatures using the enriched GO term genes ($\text{FDR} < 0.01$). The multivariate mixture model α concentration parameter was set to 5.0; the prior on the covariance matrix was set to the identity scaled by 2.0. The prior parameter for the number of clusters was set to five. We correlated hydra expression clusters with the results of the tumor microenvironment profiling tools xCell [46], CIBERSORT [47], and ESTIMATE [48]. We also applied the consensus clustering method M3C [18] and Gap statistic k-means method [49] to the TARGET MYCN-NA neuroblastoma data. We tested a range of median absolute deviation (MAD) thresholds. The number of clusters was assumed to be the smallest statistically significant value.

The hydra *sweep* command was applied to search for subtype expression within curated MSigDB gene sets. We included the hallmark ($n=50$), BioCarta ($n=289$), KEGG ($n=186$), PID ($n=196$), and Reactome (1499) genesets [16]. To increase the sensitivity for expression subtypes within well-defined signatures, we include all signatures with a minimum component probability of 10%. For example, the smallest subtype cluster considered in this analysis has 7 samples.

Small Blue Round Cell Tumor Analysis

We then compared the clustering patterns across MYCN-NA neuroblastoma, osteosarcoma, Ewing sarcoma, embryonal rhabdomyosarcoma, alveolar rhabdomyosarcoma, and synovial sarcoma. We applied the TumorMap dimensionality reduction method [5] to visualize clustering of the full small blue round cell tumor gene expression matrix. We then applied the hydra framework to explore expression variation within each disease. Each disease expression matrix had unique statistical properties including sample size and subtype variation. This required us to adapt the minimum probability threshold for each disease dataset using the *scan* routine. The Jupyter notebooks for exploring these datasets can be found on GitHub (www.github.com/jpfeil/hydra-paper/analysis). We used agglomerative clustering

to investigate patterns in the top 10 enriched gene sets for each disease's expression
279
subtypes.
280

Statistical Analysis

281

A Kruskal-Wallis test was used to identify statistically significant differences across two
282 or more groups, and a Mann-Whitney U test was used for pairwise tests using a
283 Holm-Sidak correction for multiple hypothesis testing [50,51]. We used the `scipy` [52]
284 stats implementation of the Kruskal-Wallis test and the `scikit-learn` post hoc
285 processing [53] implementation of pairwise Mann-Whitney U tests . Spearman rank and
286 Pearson correlation values were calculated using the `scipy` library [51]. Survival analysis
287 was done using the `survminer` package [54].
288

H&E Slide Preparation and Pathologist Review

289

Pediatric tumor samples were flash frozen, embedded in OCT, and 5 μ m cryosections
290 were collected. Slides were hematoxylin and eosin (H&E) stained and imaged on a Leica
291 DMi8, equipped with a HC PL APO 40x/0.85 NA objective and DFC7000T camera.
292 H&E slides were reviewed by a licensed pathologist for evidence of inflammation and
293 graded as having either minimal (< 10%) or moderate inflammation (20-30%).
294

Results

295

Performance Assessment using Synthetic Gene Expression Data

296

To assess how well hydra detects differentially expressed pathways as compared to
297 common pathway enrichment approaches, we applied these methods to
298 synthetically-generated cancer gene expression data. We generated synthetic cancer
299 gene expression data based on the TCGA glioblastoma multiforme and the MSigDB
300 Hallmark gene sets as described above. We tested a range of effect sizes and percent
301 differentially expressed genes (%DEG) within the MSigDB gene sets. We generated
302 receiver operator curves (ROC) and calculated the area under the receiver operator
303 curve (AUC) for each analysis. Overall, the hydra pipeline outperformed the
304 single-sample GSEA approaches with a mean AUC of 0.93 (95% CI: 0.91 - 0.95).
305 ssGSEA had a mean AUC of 0.72 (95% CI: 0.71 - 0.74) and GSVA had a mean AUC of
306 0.67 (95% CI: 0.66 - 0.68) (Fig 2A).
307

We further investigated the performance of these methods by plotting the AUC
308 against the effect size at 10 and 25%DEG (Fig 2B). The hydra method performed
309 better across all effect sizes, achieving near perfect performance above an effect size of
310 2.0 and 0.75 at 10 and 25%DEG, respectively. ssGSEA and GSVA performed similarly
311 at low effect sizes, but ssGSEA performed better than GSVA as the effect size increased.
312 Overall, the hydra framework performed significantly better than these standard gene
313 set enrichment approaches, particularly at low effect sizes. Therefore, the hydra
314 approach is better suited for subtyping within a disease cohort when the effect sizes are
315 smaller and fewer genes are differentially expressed.
316

0.1 Hydra Analysis of High-Risk Neuroblastoma

317

High-risk neuroblastoma is an aggressive disease and is resistant to intensive therapy.
318 Further subtyping of high-risk neuroblastoma may identify novel therapeutic targets
319 and improve risk stratification. We hypothesized that unsupervised clustering of
320 multimodally expressed genes associated with enriched Gene Ontology terms would
321 identify expression subtypes of high-risk neuroblastoma tumors. TumorMap analysis [5]
322

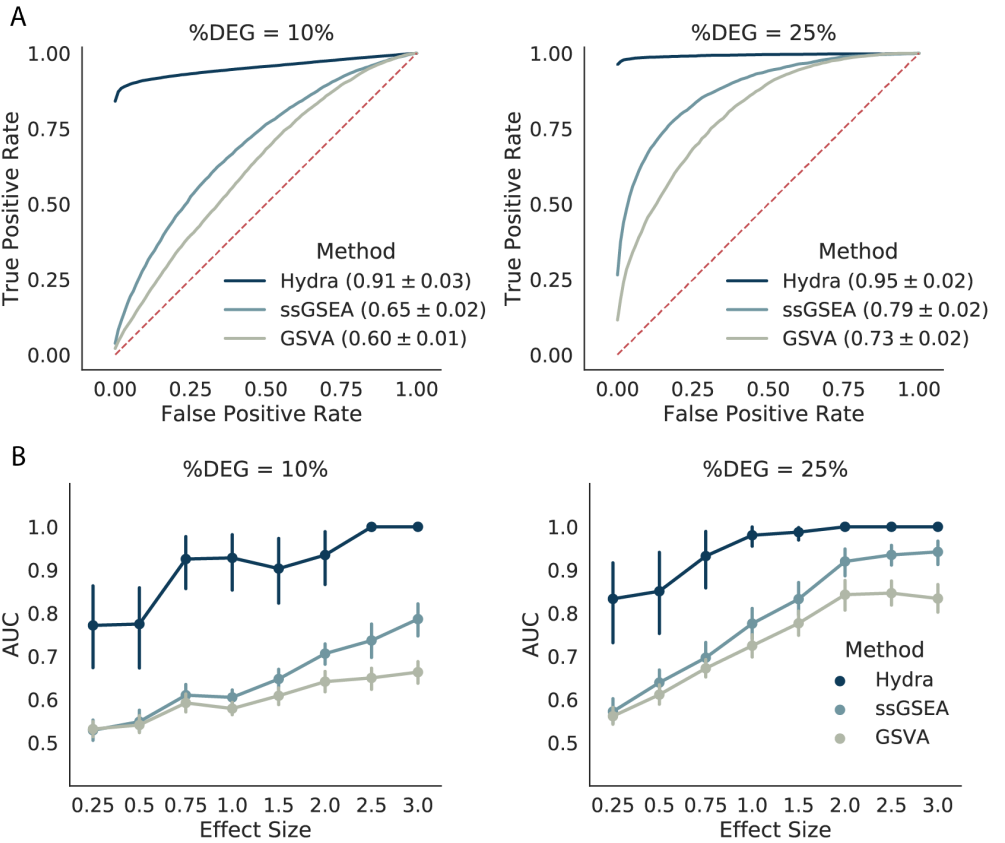


Fig 2. Hydra is more sensitive than existing gene set enrichment approaches for detecting differential pathway expression in synthetic data.
A: Mean receiver operator curves across effect sizes, percent differentially expressed genes (%DEG), and MSigDB Hallmark gene sets. A larger area under the curve (AUC) indicates better performance. The average AUC and 95% confidence interval for each method are in the ROC plot figure legends. B: Line plots comparing the mean AUC across a range of effect sizes and %DEG values.

showed that the MYCN-non-amplified (MYCN-NA) neuroblastoma samples clustered separately from MYCN-amplified (MYCN-A) and stage 4S neuroblastoma samples (S2 Fig). We focused on the MYCN-NA neuroblastoma tumor samples because this is the largest set of samples ($N=70$) and variation within MYCN-NA tumors is not well understood [55].

0.1.1 Hydra filter Analysis of High-Risk Neuroblastoma Identifies Multimodally Expressed Genes

After completing the performance assessment with synthetic gene expression data, we applied the hydra filter analysis to the TARGET high-risk neuroblastoma cohort. This analysis identified 931 genes within the MYCN-NA neuroblastoma cohort with a multimodal expression distribution. Of the 931 multimodally expressed genes, 358 genes were found to be potentially druggable by the Drug Gene Interaction Database (DGIDB) and 61 genes were associated with an FDA-approved, anti-neoplastic drug [56].

0.1.2 Hydra *sweep* Analysis of High-Risk Neuroblastoma Identifies Coordinated Expression of Multimodally Expressed Genes

Hydra *enrich* Analysis of High-Risk Neuroblastoma Identifies Distinct Tumor Microenvironment States

We applied the hydra unsupervised enrichment analysis to the MYCN-NA cohort. The multimodal expression filter identified 428 genes with a minor component probability greater than 20% (S1 File). Gene Ontology analysis found enrichment for the following GO terms (FDR: $q < 0.01$): adaptive immune response (24 genes), mesenchyme development (12 genes), steroid hormone secretion (4 genes), and response to corticosterone (4 genes). DP-GMM analysis of the 44 enriched GO term genes identified three clusters of neuroblastoma samples (Fig 3A). The posterior probability for belonging to each cluster was 42%, 34%, and 17% for clusters 1, 2, and 3, respectively. The posterior probability for a sample belonging to a new cluster was about 6% in our analysis. We next investigated cluster-specific expression signatures using GSEA (see Hydra Method section). Cluster 1 was enriched for adaptive immune response gene sets, cluster 2 was enriched for proliferative signaling gene sets, and cluster 3 was enriched for cancer-associated fibroblast gene sets (Fig 3B). Cluster 3 shares several features of a wound healing response, including fibroblast recruitment, extracellular matrix organization, and infiltration of immune cells [57].

Clusters 1 and 3 were enriched for tumor microenvironment-associated gene expression. To further validate this signal, we correlated the hydra clusters with enrichment scores from the tumor microenvironment profiling tools xCell [46] and ESTIMATE [48]. Cluster 1 had high average xCell enrichment scores associated with adaptive immune cell types including B-cells, CD4+ naive T-cells, and CD8+ naive T-cells (Kruskal-Wallis: $p < 0.001$). Cluster 2 was characterized by the absence of immune and stromal expression and higher tumor purity scores than clusters 1 and 3. The average ESTIMATE tumor purity was 88%, 96% and 82% for clusters 1, 2, and 3, respectively. Cluster 3 was enriched for fibroblast-associated expression by xCell analysis (Kruskal-Wallis: $p < 0.001$). Clusters 1 and 3 had higher ESTIMATE immune-associated expression levels than cluster 2 (average ImmuneScore per cluster: 58, -612, 56), but cluster 3 had the highest stromal expression signature score (average StromalScore per cluster: -1027, -1310, -135). Comparing ESTIMATE enrichment scores across clusters reveals clear trends in broad immune and stromal expression signatures.

We next correlated clusters with clinical features. We found no difference in patient survival outcomes across clusters (log-rank test, $p > 0.05$). Notably, cluster 1, which had the highest adaptive immune expression signal in MYCN-NA neuroblastoma, over-expresses cell-cycle regulation genes, which was not observed in other small blue cell tumors. We investigated associations with clinical covariates mutation burden, age, and tumor content as assessed by a clinical pathologist, but found no statistically significant differences (Kruskal-Wallis: $p > 0.05$). We then investigated associations between the hydra clusters and neuroblastoma-associated molecular aberrations and clinical features (Supplementary Table 6). ATRX gene deletions were enriched in cluster 1 (Fisher's Exact Test: $p < 0.05$). MKI low tumors were enriched in cluster 2 and 3 (Fisher's Exact Test: $p < 0.01$). Chromosome 17 wild-type tumors were enriched in clusters 2 and 3 (Fisher's Exact Test: $p < 0.01$). Analysis on a larger dataset may reveal additional clusters and correlations with clinical features.

Consensus clustering is a widely used approach for identifying tumor subtypes using gene expression data. We applied the M3C consensus clustering method, which is a more sophisticated version of consensus clustering that uses a null distribution to assess the statistical significance of the clustering [18,19]. We used the top 5000 genes with the largest median absolute deviation (MAD) because this threshold is routinely used in

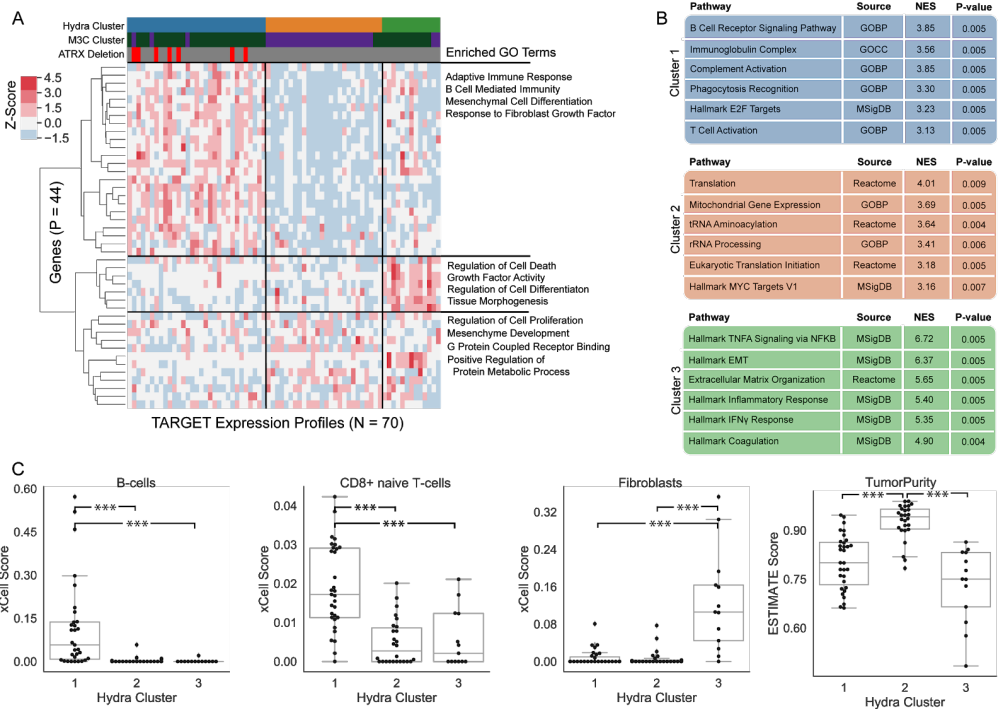


Fig 3. Hydra analysis identifies three distinct tumor microenvironment expression subtypes in MYCN non-amplified neuroblastoma samples. A: Gene expression heatmap displaying expression profiles of hydra clusters. Heatmap columns (samples) are ordered by hydra cluster membership. Ward hierarchical clustering applied to rows (genes) identified coordinated expression of GO term genes. These GO term genes were originally identified by the hydra *enrich* command. B: GSEA performed on each cluster identified enrichment of tumor microenvironment and proliferative signaling gene sets. C: xCell enrichment score distributions for B-cells, CD8+ naive T-cells, and Fibroblasts, and the ESTIMATE TumorPurity score distributions for each cluster; enrichments for all cell types are available in S1 File. Abbreviations: Normalized Enrichment Score (NES), Epithelial to Mesenchymal Transition (EMT), Gene Ontology Biological Process (GOBP).

unsupervised clustering of cancer gene expression data [58–60]. The M3C analysis resulted in the identification of two statistically significant clusters. One M3C cluster correlated with hydra clusters 1 and 3 and the other M3C cluster correlated with hydra cluster 2. Therefore, M3C clustering detected the tumor purity signal in the expression data, but was not able to separate the adaptive immune cell and fibroblast infiltrated clusters (hydra clusters 1 and 3). We also applied k-means clustering using the gap statistic approach [49,61] for estimating the number of clusters, but this approach grouped all samples into a single cluster. We tested a range of MAD thresholds based on the median absolute deviation, but found similar results across thresholds (S3 Fig). Overall, the hydra approach was more sensitive at detecting distinct tumor microenvironment states than these other popular clustering methods.

N-of-1 Tumor Analysis for Pediatric Neuroblastoma

We investigated the predictive performance of the hydra approach for identifying clinically relevant signals in the N-of-1 tumor analysis setting. The command-line

interface of the hydra toolkit includes a *predict* function for labeling samples using a pre-fit model. The MYCN-NA neuroblastoma model described above was used to predict expression subtypes on a new set of samples. We obtained tumor gene expression data from five stage 4, MYCN-NA neuroblastoma samples from the UCSC Treehouse gene expression compendium [5, 6]. The age at diagnosis ranged from 2 to 6 years. Four out of five samples had a deletion in the ATRX gene. Samples 1D and 1R were diagnosis and resection samples from the same patient. Most of the samples (4 out of 5) clustered in cluster 1, which is characterized by adaptive immune pathway expression.

Three of the ATRX-deleted samples clustered with the high immune expression cluster (cluster 1) and one clustered in the low immune, high proliferative signaling cluster (cluster 2). Hydra analysis assigned sample 1D to cluster 1 and sample 1R to cluster 2 despite both samples originating from the same patient. The resection sample 1R was extracted from lymph node tissue, which has a significantly different cellular composition than the training data. Another possible explanation for the different cluster assignments is that the tumor microenvironment is dynamic and the tumor may evade immune recognition as the disease progresses, resulting in different expression signatures. We performed GSEA comparing samples 1D and 1R to investigate potential mechanisms leading to immune evasion in sample 1R. GSEA found downregulation of the MHC Class I Antigen Processing & Presentation GO term in sample 1R (adjusted p-value < 0.002). Loss of antigen processing functions is a common mechanism of immune evasion across cancer types [62].

H&E slide images for the 5 MYCN-NA neuroblastomas were reviewed by a licensed pathologist and scored for evidence of inflammation. The hydra analysis agreed with the pathologist review in 4 out of 5 samples, with sample 4 as the one discordant sample (Fig 4). Sample 4 is from lymph node tissue, which may have inherently high immune expression because the lymph nodes normally contain lymphocytes. Small round blue cell tumors are also difficult to differentiate from immune cells because these cell types share histological features. Notably, concordant ESTIMATE values were present in 3 out of 5 samples scored by the pathologist: samples 1D, 1R, and 2.

To further investigate expression patterns within the hydra-identified tumor microenvironment subtypes, we performed GSEA by z-score normalizing each tumor's gene expression data to its tumor microenvironment cluster. This is a novel GSEA approach that uses the tumor microenvironment state discovered by the hydra method to identify additional gene expression signals for individual samples. This approach revealed signals not present at the cohort level analysis (S4 Fig). For example, enrichment of immune expression signatures within cluster 2 predicted differences in overall survival such that patients with higher immune expression had a better overall survival rate. Similarly, an elevated cell cycle signal within cluster 3 predicted worse survival compared to other cluster 3 samples with lower cell cycle expression. A metastatic expression signal was identified in the analysis of cluster 1 samples, but this signature did not correlate with a difference in survival. This approach may therefore provide a more appropriate background distribution for revealing and evaluating the significance of gene expression patterns and survival statistics within tumor subtypes.

Hydra Analysis Discovers Complex Tissue Signatures

While the MYCN-NA neuroblastoma analysis above focused on immune and fibroblast expression signatures, the hydra *enrich* method is unsupervised and can therefore detect any type of expression signature. To illustrate this, we applied the hydra *filter/enrich* analysis to the TARGET osteosarcoma cohort (N=74) and discovered enrichment of the GO striated muscle contraction term (FDR < 0.01, S5 Fig). Multivariate clustering for the GO striated muscle contraction gene set using the sweep routine identified two clusters. xCell analysis of the osteosarcoma cohort found significant enrichment of

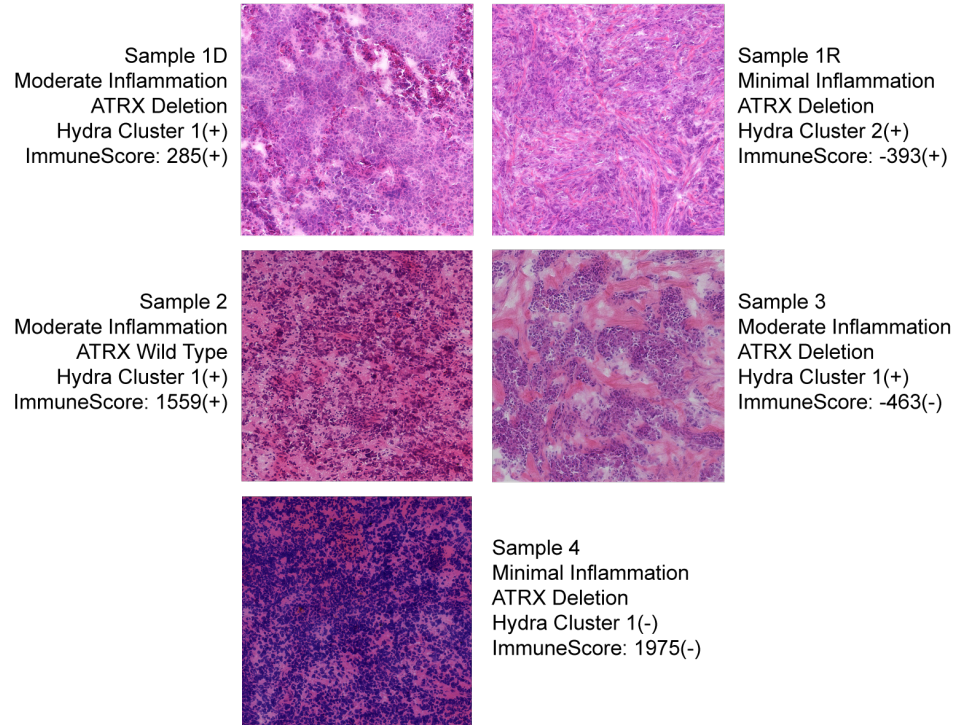


Fig 4. Hydra method correlates with histopathology review of tumor H&E slides. The tumor microenvironments of stage 4 MYCN-NA neuroblastoma patient samples were analyzed using gene expression and H&E slide image data. Inflammation levels in the same tumor samples were assessed from H&E slide images at 20x magnification (Moderate inflammation: 20-30% lymphocyte content; Minimal inflammation: < 10% lymphocyte content). ATRX mutation status, hydra cluster assignment, and ESTIMATE ImmuneScore value are also indicated. Concordant and discordant predictions are marked with a positive (+) and negative (-) sign, respectively.

skeletal muscle expression in the second cluster (Mann-Whitney U test, $p < 0.001$). Surprisingly, the M3C clustering approach was not able to detect the strong muscle signature using the 5000 genes with the largest MAD ($p > 0.05$). We used the muscle expression signature to identify osteosarcoma tumors in the Treehouse Compendium which also contained a similar expression signature. We subsequently confirmed with a licensed pathologist that one of the muscle-expression positive tumor samples did contain significant muscle tissue infiltration. This analysis is completely unsupervised and revealed expression signatures not routinely investigated but contributes significantly to the tumor expression profile. Explaining these sources of variation is necessary to derive clinically relevant conclusions from gene expression data.

We applied the *filter* method to Ewing sarcoma and discovered multimodal expression of a druggable gene, JAK1. Applying the multimodal expression model allowed us to deconstruct the Ewing sarcoma distribution into three components. We found that the expression component with the highest JAK1 expression was also enriched for mast cell expression (S6 Fig). Therefore, over-expression of JAK1 may not correspond to activation of the JAK/STAT signaling pathway in cancer cells but rather to the presence of mast cells within the tumor microenvironment. Furthermore, targeted inhibition of JAK1 using ruxolitinib was shown to inhibit essential mast cell functions, including degranulation [63]. Therefore, therapeutic intervention intending to inhibit JAK1 expression in cancer cells may inadvertently inhibit the patient's mast cell

functions. Over-expression analysis using the Ewing sarcoma JAK1 expression distribution may identify JAK1 as an actionable lead, but further investigation into the effect of inhibiting off-target JAK1 expression in mast cells is needed. The hydra framework facilitates the identification of important expression signatures which can be used to deconstruct complex tumor expression subtypes and identify potentially confounding expression signals.

Hydra Analysis Reveals Similar Expression Subtypes Across Pediatric Cancers

We next investigated whether similar hydra clusters could be identified across other small blue round cell tumors. We first performed TumorMap analysis, which is a dimensionality reduction approach for visualizing genomic data on a 2D surface [5]. We found that small blue round cell tumor types — MYCN-NA neuroblastoma, osteosarcoma, Ewing sarcoma, synovial sarcoma, alveolar rhabdomyosarcoma, and embryonal rhabdomyosarcoma — all form separate TumorMap clusters (Fig 5A). This suggests there is a strong cell-of-origin signal driving the clustering of these cancer types, which is an observation that was recently made in the larger TCGA dataset of adult cancers [64]. While pan-cancer analysis emphasized the differences across small blue round cell tumors, we hypothesized that expression subtypes within histological cancer types would share similar biological themes.

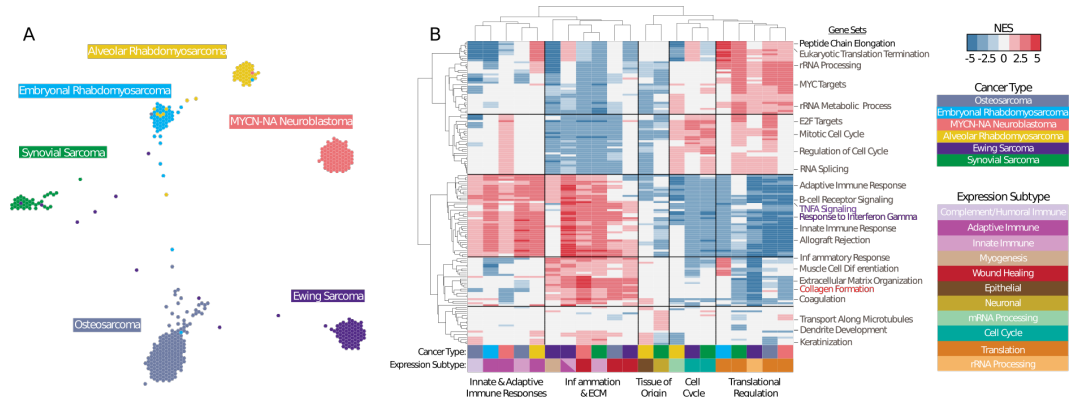


Fig 5. Hydra analysis of small blue round cell tumors reveals similar expression subtypes across cancer types. A: TumorMap visualization of 6 small blue round cell tumor types. B: Hierarchically clustered heatmap for the top 10 enriched gene sets across the 21 small blue round cell tumor expression subtypes. Each column corresponds to a cancer type and an expression subtype (x-axis). Each row corresponds to a gene set. The expression subtype was manually assigned after reviewing the most highly enriched gene sets for each cancer expression subtype.

We next performed hydra analysis within each cancer type and were surprised to find shared biological themes across all six small blue round tumor types. Hierarchical clustering of the top 10 statistically significant gene sets for each disease cluster resulted in clustering of diseases by expression subtype and not the cancer histology (Fig 5B). Common themes emerged across diseases including translational regulation, cell cycle regulation, immune effector cell signaling, inflammation, extracellular matrix organization, and tissue-of-origin signals. Furthermore, these signals predicted differences in patient outcomes in osteosarcoma and synovial sarcoma (S6 Fig). In both cases, the presence of immune associated expression correlated with better patient outcomes compared to tumors with proliferative signaling pathways associated with the

upregulation of translation initiation. Survival data were not available for the rhabdomyosarcoma and Ewing sarcoma expression datasets.

501
502

Discussion

503

The hydra framework uses model-based clustering to facilitate the discovery of recurrent expression patterns within cancer gene expression cohorts. We leveraged recent improvements in model-based clustering algorithms to identify differentially expressed genes without a matched normal distribution. We modeled differential expression as a multimodal Gaussian distribution using nonparametric Bayesian statistics. We then enriched for biologically-annotated Gene Ontology terms and performed multivariate clustering to reveal expression subtypes. The hydra framework can be used for both identifying expression subtypes within large cohorts and classifying new tumor gene expression profiles using the trained models. The hydra framework outperformed standard gene set enrichment tools for identifying overexpression of the MSigDB Hallmark cancer gene sets in synthetic data. Application of this framework to small blue round cell tumors identified shared biological themes associated with the tumor microenvironment.

504
505
506
507
508
509
510
511
512
513
514
515
516

Multivariate gene expression analysis is typically underpowered because the number of genes greatly exceeds the number of samples. To address this limitation, we propose selecting for multimodally expressed genes before performing multivariate analysis. The hydra multimodal filter reduces the number of genes and enriches for genes that participate in known biological processes, including those curated in the Gene Ontology database. For example, multimodally expressed genes separate neuroblastoma subtypes by TumorMap analysis better than the standard approach of using all expressed genes. Furthermore, we showed that the hydra approach is more sensitive at resolving tumor microenvironment subtypes than the M3C consensus clustering and k-means gap-statistic approach.

517
518
519
520
521
522
523
524
525
526

Significant progress has been made in subtyping neuroblastomas and adapting therapy for aggressive subtypes, but unexplained heterogeneity remains [55]. Failure to account for this heterogeneity decreases the power of standard methods to detect important expression patterns. Identifying biomarkers using genome-wide technology may lead to improved risk stratification and the discovery of novel drug targets. Hydra analysis of the TARGET MYCN-NA neuroblastoma cohort ($N=70$) found differential expression of tumor microenvironment markers, including markers of the adaptive immune response. Pediatric cancers are generally thought to be less immunogenic because they have lower mutation burdens than adult cancers, but the immunogenicity of pediatric cancer has not been sufficiently investigated [65]. Our analysis found significant variation in immune marker expression and identified ATRX deletions as a potential biomarker of immune infiltrated tumors in MYCN-NA neuroblastoma. Analysis of other small blue round cell tumors revealed similar expression signatures across tumor types, despite samples clustering by their histology in a pan-cancer TumorMap analysis. Identification of shared expression signatures across cancer types may suggest that these patients would respond similarly to therapies that target these pathways. In particular, the identification of a cross-disease subtype associated with high expression of immune markers may warrant further investigation of immunotherapies in small blue round cell tumors using a basket clinical trial design [66].

527
528
529
530
531
532
533
534
535
536
537
538
539
540
541
542
543
544
545
546
547
548
549
550

We found significant differences in immune and stromal expression that may inform precision medicine applications. The tumor microenvironment has become an important therapeutic consideration, but few methods account for the tumor microenvironment directly. Tumor purity has been identified as a confounding factor in cancer gene expression subtyping efforts [67]. For example, tumor purity and tumor

microenvironment expression have been shown to correlate with pancreatic cancer
551 subtypes [68]. Furthermore, Aran et al. (2018) found that tumor purity was correlated
552 with the mesenchymal glioblastoma subtype and recommended a differential expression
553 approach to computationally remove the tumor purity signal. However, standard
554 approaches for subtracting the tumor purity effect may not be the best approach
555 because several mechanisms may influence tumor purity, and each mechanism may
556 result in a different expression pattern. For instance, our analysis of MYCN-NA
557 neuroblastoma identified two gene expression signatures that correlated with lower
558 predicted tumor purity. Cluster 1 had an adaptive immune expression signature and
559 cluster 3 had a cancer-associated fibroblast signature. Therefore, we suggest that the
560 estimated tumor purity signal should not be subtracted without first accounting for the
561 different mechanisms influencing tumor purity.
562

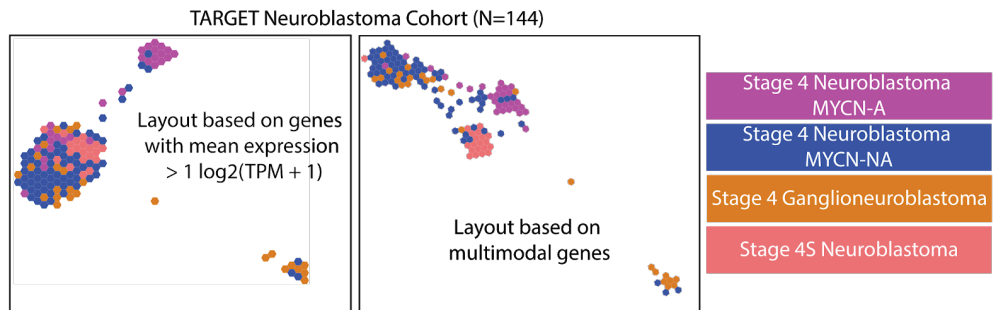
We also found shared biological pathway enrichment across small blue round cell
563 tumors. Although these diseases have distinct expression patterns on the surface, we
564 discovered common themes once we accounted for the cell-of-origin signal. There appear
565 to be at least three major tumor microenvironment states: immune silent, immune
566 infiltrated, and wound healing subtypes. The immune infiltrated and wound healing
567 subtypes predicted better overall survival in osteosarcoma and delayed metastases in
568 synovial sarcoma tumors, which suggests the involvement of the host immune response
569 limits the progression of tumors. Amplification of the host immune response may
570 further limit tumor growth and lead to immune-mediated tumor cell death.
571

Conclusion

Precision oncology aims to differentiate tumors of the same diagnosis in order to match
572 patients with the best treatment. We have developed the hydra framework to discover
573 subtle but recurrent expression patterns within a cohort of samples with the same
574 diagnosis, which is a novel strategy for pediatric precision oncology research. Our
575 approach may help to uncover the biology underlying tumor progression and response to
576 therapy. We have shown that hydra is more sensitive than standard gene set enrichment
577 approaches for detecting differential pathway expression. Additionally, our framework
578 provides tools to conduct unsupervised clustering analysis to discover expression
579 subtypes. We applied the unsupervised hydra analysis to small blue round cell tumors
580 and discovered distinct tumor microenvironment states. This shows that one of the
581 strongest signals in clinical gene expression data comes from the TME, so careful
582 modeling of the TME is required to maximize the impact of clinical gene expression
583 analysis. The hydra framework provides unbiased clustering tools to characterize these
584 sources of variation in specific disease populations and identify shared biological themes
585 that can potentially be targeted therapeutically.
586

Supporting information

S1 Fig. Example of bnpv memoized online variational inference clustering on toy data. We used the bnpv moVB algorithm to infer the number of clusters from synthetic data. The model first randomly assigns clusters. Then, the model iteratively improves the model fit, creating and destroying clusters until the model converges on the correct number of clusters [34].
588
589
590
591
592
593

S2 Fig.

595

596

597

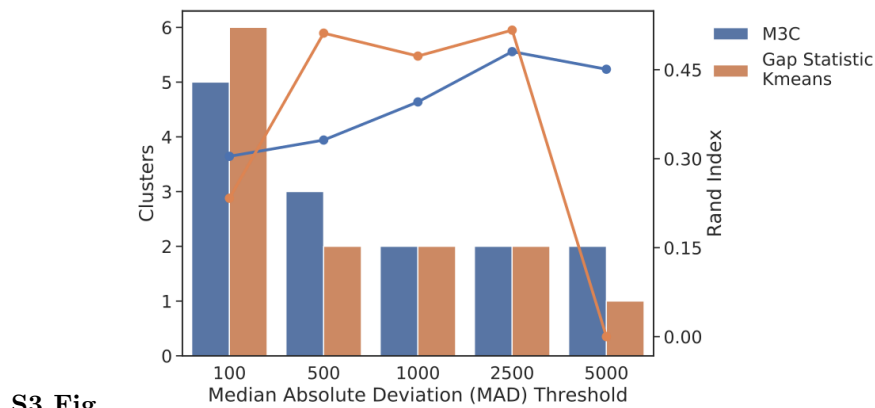
598

599

600

601

Enriching for multimodally expressed genes improves clustering of established neuroblastoma subtypes. Standard TumorMap analysis (Newton et al. 2017) of the TARGET neuroblastoma dataset resulted in stage 4S samples clustering with stage 4 neuroblastoma samples (left). An alternative TumorMap based solely on 1,498 multimodally expressed genes separated the stage 4S samples into a distinct cluster (right).



602

603

604

605

606

607

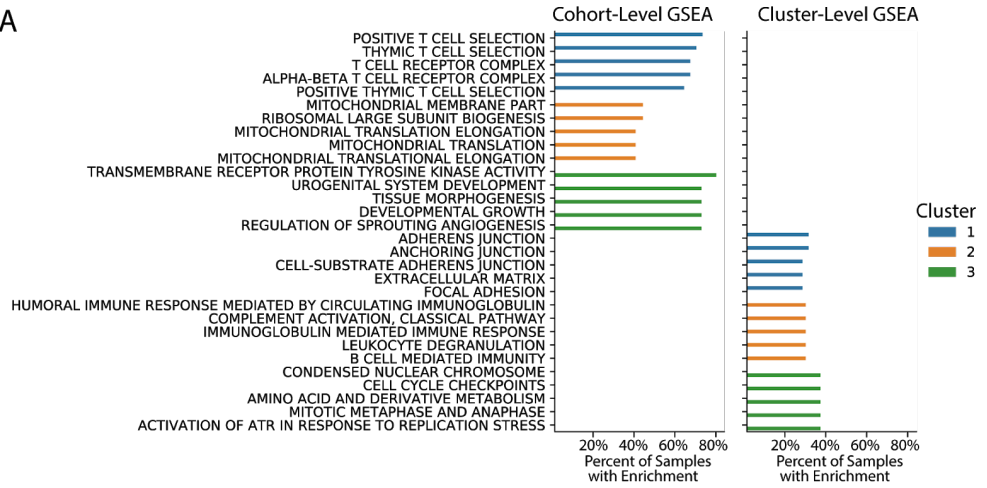
608

S3 Fig.

Consensus and k-means clustering applied to TARGET MYCN-NA dataset. We tested a range of gene expression variation thresholds based on the median absolute deviation, but found that the clusters identified by this approach could not resolve the same clusters as the hydra approach. The barplot shows the number of clusters and the lineplot tracks the Rand index comparing the M3C and k-means clusters and the hydra clusters.

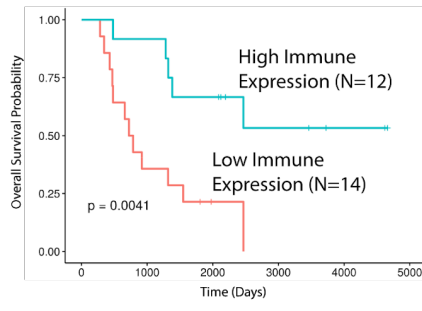
S4 Fig.

A



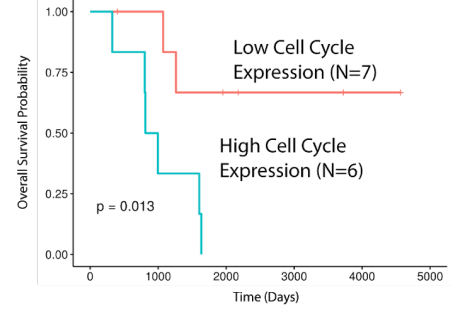
B

Cluster 2 Immune Analysis



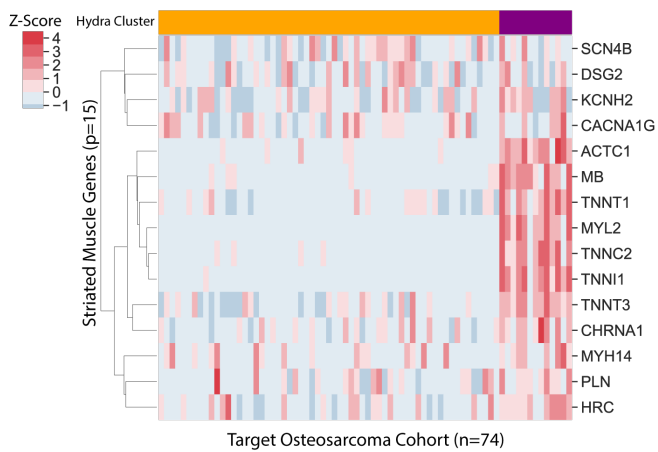
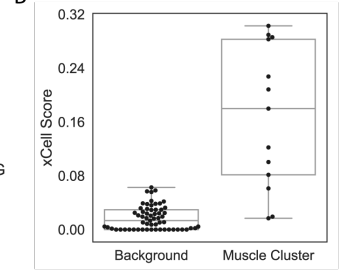
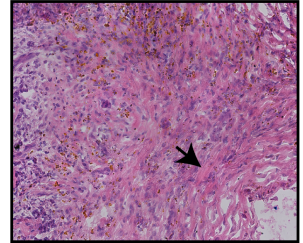
C

Cluster 3 Cell Cycle Analysis

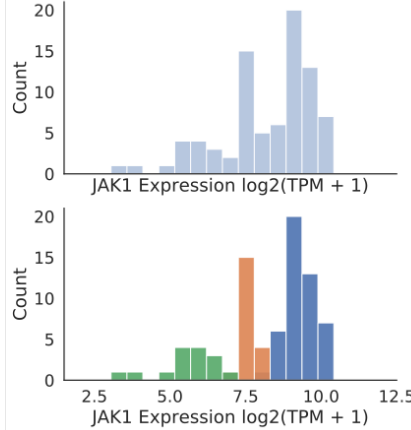
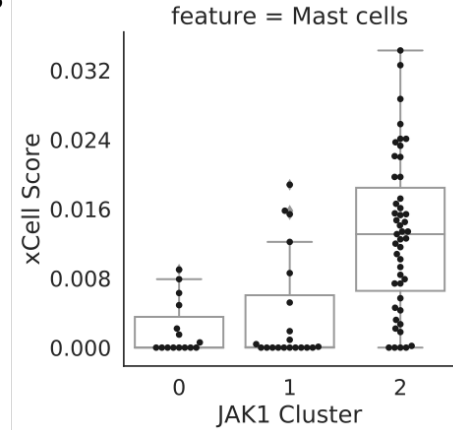


Gene set enrichment analysis (GSEA) of MYCN-NA neuroblastoma identifies survival differences within hydra cluster 2 and cluster 3. A: Top 5 differentially enriched gene sets for each cluster comparing the entire MYCN-NA neuroblastoma cohort (cohort-level GSEA) and the corresponding hydra cluster (cluster-level GSEA). GSEA analysis of the hydra clusters found immune and cell cycle signals that were not identified in the cohort-level analysis. B: cluster-level GSEA separated cluster 2 into high and low immune subtypes. C: cluster-level GSEA separated cluster 3 into high and low cell cycle subtypes.

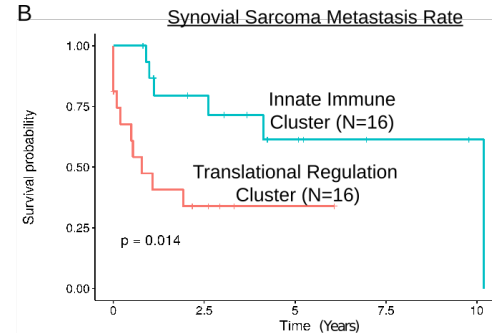
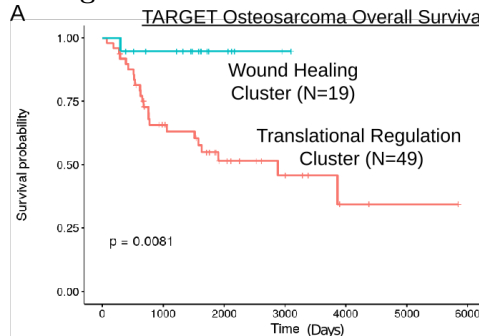
610
611
612
613
614
615
616
617
618

S5 Fig.**A****B****C**

Hydra analysis of TARGET osteosarcoma cohort reveals skeletal muscle signature. Hydra enrichment analysis on the TARGET osteosarcoma cohort revealed a subset of patients with high skeletal muscle expression. A: Clustered heatmap shows the muscle signature genes identified by hydra unsupervised enrichment analysis. B: xCell tumor microenvironment profiling identified significant differences in skeletal muscle expression compared to background ($p < 0.001$). C: H&E stained tumor slide for an independent osteosarcoma sample confirms presence of striated muscle tissue within the sequenced tumor sample.

S6 Fig.**A****B**

Hydra analysis identifies correlation between expression of druggable JAK1 gene and mast cell expression signature in Ewing sarcoma. A: We show the utility of the mixture model approach for identifying important gene expression patterns for precision medicine applications. JAK1 is a druggable gene, but JAK1 is also an important gene in immune cell signaling pathways. B: Boxplot showing the xCell mast cell enrichment score for three clusters associated with JAK1 expression.

S7 Fig.

Hydra analysis identifies tumor microenvironment expression subtypes that correlate with patient outcomes in osteosarcoma and synovial sarcoma.
A: Kaplan-Meier plot showing overall survival curves for osteosarcoma wound healing and translation clusters. B: Kaplan-Meier plot showing metastasis survival curves for synovial sarcoma innate immune and translation clusters.

S1 File. TARGET MYCN-NA Neuroblastoma Supplementary Data.

Acknowledgments

We would like to thank the patients and families who participated in translational genomics research. We would also like to thank St. Baldrick's Foundation, California Precision Medicine Initiative, National Human Genome Research Institute of the National Institutes of Health for funding support.

References

1. Vivian J, Rao AA, Nothaft FA, Ketchum C, Armstrong J, Novak A, et al. Toil Enables Reproducible, Open Source, Big Biomedical Data Analyses;35(4):314–316. doi:10.1038/nbt.3772.
2. Pugh TJ, Morozova O, Attiyeh EF, Asgharzadeh S, Wei JS, Auclair D, et al. The Genetic Landscape of High-Risk Neuroblastoma;45(3):279–284. doi:10.1038/ng.2529.
3. Goldman M, Craft B, Kamath A, Brooks A, Zhu J, Haussler D. The UCSC Xena Platform for Cancer Genomics Data Visualization and Interpretation; p. 326470. doi:10.1101/326470.
4. The Cancer Genome Atlas Research Network, Weinstein JN, Collisson EA, Mills GB, Shaw KRM, Ozenberger BA, et al. The Cancer Genome Atlas Pan-Cancer Analysis Project;45:1113–1120. doi:10.1038/ng.2764.
5. Newton Y, Novak AM, Swatloski T, McColl DC, Chopra S, Graim K, et al. TumorMap: Exploring the Molecular Similarities of Cancer Samples in an Interactive Portal;77(21):e111–e114. doi:10.1158/0008-5472.CAN-17-0580.
6. Vaske OM, Bjork I, Salama SR, Beale H, Shah AT, Sanders L, et al. Comparative Tumor RNA Sequencing Analysis for Difficult-to-Treat Pediatric and Young Adult Patients With Cancer;2(10):e1913968–e1913968. doi:10.1001/jamanetworkopen.2019.13968.

7. Joyce JA, Fearon DT. T Cell Exclusion, Immune Privilege, and the Tumor Microenvironment;348(6230):74–80. doi:10.1126/science.aaa6204.
8. Chen DS, Mellman I. Elements of Cancer Immunity and the Cancer–Immune Set Point;541(7637):321–330. doi:10.1038/nature21349.
9. Mellman I, Coukos G, Dranoff G. Cancer Immunotherapy Comes of Age;480(7378):480–489. doi:10.1038/nature10673.
10. Page DB, Postow MA, Callahan MK, Allison JP, Wolchok JD. Immune Modulation in Cancer with Antibodies;65:185–202. doi:10.1146/annurev-med-092012-112807.
11. Anders S, McCarthy DJ, Chen Y, Okoniewski M, Smyth GK, Huber W, et al. Count-Based Differential Expression Analysis of RNA Sequencing Data Using R and Bioconductor;8(9):1765–1786. doi:10.1038/nprot.2013.099.
12. Anders S, Huber W. Differential Expression Analysis for Sequence Count Data;11(10):R106. doi:10.1186/gb-2010-11-10-r106.
13. Soneson C, Delorenzi M. A Comparison of Methods for Differential Expression Analysis of RNA-Seq Data;14(1):91. doi:10.1186/1471-2105-14-91.
14. Subramanian A, Tamayo P, Mootha VK, Mukherjee S, Ebert BL, Gillette MA, et al. Gene Set Enrichment Analysis: A Knowledge-Based Approach for Interpreting Genome-Wide Expression Profiles;102(43):15545–15550. doi:10.1073/pnas.0506580102.
15. Mootha VK, Lindgren CM, Eriksson KF, Subramanian A, Sihag S, Lehar J, et al. PGC-1alpha-Responsive Genes Involved in Oxidative Phosphorylation Are Coordinately Downregulated in Human Diabetes;34(3):267–273. doi:10.1038/ng1180.
16. Liberzon A, Subramanian A, Pinchback R, Thorvaldsdóttir H, Tamayo P, Mesirov JP. Molecular Signatures Database (MSigDB) 3.0;27(12):1739–1740. doi:10.1093/bioinformatics/btr260.
17. Oyelade J, Isewon I, Oladipupo F, Aromolaran O, Uwoghiren E, Ameh F, et al. Clustering Algorithms: Their Application to Gene Expression Data;10:237–253. doi:10.4137/BBI.S38316.
18. John CR, Watson D, Russ D, Goldmann K, Ehrenstein M, Lewis M, et al. M3C: A Monte Carlo Reference-Based Consensus Clustering Algorithm; p. 377002.
19. Wilkerson MD, Hayes DN. ConsensusClusterPlus: A Class Discovery Tool with Confidence Assessments and Item Tracking;26(12):1572–1573. doi:10.1093/bioinformatics/btq170.
20. Lenz M, Müller FJ, Zenke M, Schuppert A. Principal Components Analysis and the Reported Low Intrinsic Dimensionality of Gene Expression Microarray Data;6(1):1–11. doi:10.1038/srep25696.
21. Yi Li, Wing-Kin Sung, Miller LD. Multimodality as a Criterion for Feature Selection in Unsupervised Analysis of Gene Expression Data. In: Fifth IEEE Symposium on Bioinformatics and Bioengineering (BIBE’05);. p. 276–280.
22. Ghosh D. Mixture Models for Assessing Differential Expression in Complex Tissues Using Microarray Data;20(11):1663–1669. doi:10.1093/bioinformatics/bth139.

23. Dahl DB, Vannucci M. In: Do KA, Muller P, editors. Model-Based Clustering for Expression Data via a Dirichlet Process Mixture Model. Cambridge University Press; p. 201–218. Available from: https://www.cambridge.org/core/product/identifier/CB09780511584589A070/type/book_part.
24. Kim S, Tadesse MG, Vannucci M. Variable Selection in Clustering via Dirichlet Process Mixture Models;93(4):877–893. doi:10.1093/biomet/93.4.877.
25. Gelman A, Carlin JB, Stern HS, Dunson DB, Vehtari A, Rubin DB, et al. Bayesian Data Analysis. Chapman and Hall/CRC;. Available from: <https://www.taylorfrancis.com/books/9780429113079>.
26. Thall PF, Mueller P, Xu Y, Guindani M. Bayesian Nonparametric Statistics: A New Toolkit for Discovery in Cancer Research;16(6):414–423. doi:10.1002/pst.1819.
27. Teh YW. Dirichlet Process; p. 280–287.
28. Antoniak CE. Mixtures of Dirichlet Processes with Applications to Bayesian Nonparametric Problems;2(6):1152–1174. doi:10.1214/aos/1176342871.
29. Ferguson TS. A Bayesian Analysis of Some Nonparametric Problems;1(2):209–230. doi:10.1214/aos/1176342360.
30. Müller P, Quintana FA. Nonparametric Bayesian Data Analysis; p. 95–110.
31. Görür D, Edward Rasmussen C. Dirichlet Process Gaussian Mixture Models: Choice of the Base Distribution;25(4):653–664. doi:10.1007/s11390-010-9355-8.
32. Hughes MC, Sudderth E. Memoized Online Variational Inference for Dirichlet Process Mixture Models. In: Advances in Neural Information Processing Systems; p. 1133–1141.
33. Neal RM. Markov Chain Sampling Methods for Dirichlet Process Mixture Models;9(2):249–265. doi:10.1080/10618600.2000.10474879.
34. Hughes MC, Sudderth EB. Bnpy : Reliable and Scalable Variational Inference for Bayesian Nonparametric Models; p. 4.
35. Ashburner M, Ball CA, Blake JA, Botstein D, Butler H, Cherry JM, et al. Gene Ontology: Tool for the Unification of Biology;25(1):25–29. doi:10.1038/75556.
36. Consortium GO. The Gene Ontology Resource: 20 Years and Still GOing Strong;47(D1):D330–D338.
37. Merico D, Isserlin R, Stueker O, Emili A, Bader GD. Enrichment Map: A Network-Based Method for Gene-Set Enrichment Visualization and Interpretation;5(11):e13984.
38. Yu G, Wang LG, Han Y, He QY. clusterProfiler: An R Package for Comparing Biological Themes among Gene Clusters;16(5):284–287. doi:10.1089/omi.2011.0118.
39. Tamayo P, Steinhardt G, Liberzon A, Mesirov JP. The Limitations of Simple Gene Set Enrichment Analysis Assuming Gene Independence;25(1):472–487. doi:10.1177/0962280212460441.
40. Korotkevich G, Sukhov V, Sergushichev A. Fast Gene Set Enrichment Analysis; p. 060012. doi:10.1101/060012.

41. Barbie DA, Tamayo P, Boehm JS, Kim SY, Moody SE, Dunn IF, et al. Systematic RNA Interference Reveals That Oncogenic KRAS-Driven Cancers Require TBK1;462(7269):108–112. doi:10.1038/nature08460.
42. Hänelmann S, Castelo R, Guinney J. GSVA: Gene Set Variation Analysis for Microarray and RNA-Seq Data;14(1):7. doi:10.1186/1471-2105-14-7.
43. Tarca AL, Bhatti G, Romero R. A Comparison of Gene Set Analysis Methods in Terms of Sensitivity, Prioritization and Specificity;8(11):e79217. doi:10.1371/journal.pone.0079217.
44. Zwiener I, Frisch B, Binder H. Transforming RNA-Seq Data to Improve the Performance of Prognostic Gene Signatures;9(1):e85150. doi:10.1371/journal.pone.0085150.
45. Lagarde P, Przybyl J, Brulard C, Pérot G, Pierron G, Delattre O, et al. Chromosome Instability Accounts for Reverse Metastatic Outcomes of Pediatric and Adult Synovial Sarcomas;31(5):608–615. doi:10.1200/JCO.2012.46.0147.
46. Aran D, Hu Z, Butte AJ. xCell: Digitally Portraying the Tissue Cellular Heterogeneity Landscape;18(1):220. doi:10.1186/s13059-017-1349-1.
47. Newman AM, Liu CL, Green MR, Gentles AJ, Feng W, Xu Y, et al. Robust Enumeration of Cell Subsets from Tissue Expression Profiles;12(5):453–457. doi:10.1038/nmeth.3337.
48. Yoshihara K, Shahmoradgoli M, Martínez E, Vegesna R, Kim H, Torres-Garcia W, et al. Inferring Tumour Purity and Stromal and Immune Cell Admixture from Expression Data;4:2612. doi:10.1038/ncomms3612.
49. Tibshirani R, Walther G, Hastie T. Estimating the Number of Clusters in a Data Set via the Gap Statistic;63(2):411–423.
50. Pedregosa F, Varoquaux G, Gramfort A, Michel V, Thirion B, Grisel O, et al. Scikit-Learn: Machine Learning in Python;12:2825–2830.
51. Jones E, Oliphant T, Peterson P, et al. SciPy: Open Source Scientific Tools for Python;.
52. Virtanen P, Gommers R, Oliphant TE, Haberland M, Reddy T, Cournapeau D, et al. SciPy 1.0—Fundamental Algorithms for Scientific Computing in Python; p. arXiv:1907.10121.
53. Terpilowski M. Scikit-Posthocs: Pairwise Multiple Comparison Tests in Python;4(36):1169. doi:10.21105/joss.01169.
54. Kassambara A, Kosinski M, Biecek P. Survminer: Drawing Survival Curves Using ‘Ggplot2’;. Available from: <https://CRAN.R-project.org/package=survminer>.
55. Morgenstern DA, Bagatell R, Cohn SL, Hogarty MD, Maris JM, Moreno L, et al. The Challenge of Defining “Ultra-High-Risk” Neuroblastoma;66(4):e27556. doi:10.1002/pbc.27556.
56. Cotto KC, Wagner AH, Feng YY, Kiwala S, Coffman AC, Spies G, et al. DGIdb 3.0: A Redesign and Expansion of the Drug–Gene Interaction Database;46(D1):D1068–D1073.

57. Foster DS, Jones RE, Ransom RC, Longaker MT, Norton JA. The Evolving Relationship of Wound Healing and Tumor Stroma;3(18). doi:10.1172/jci.insight.99911.
58. Bourgon R, Gentleman R, Huber W. Independent Filtering Increases Detection Power for High-Throughput Experiments;107(21):9546–9551. doi:10.1073/pnas.0914005107.
59. Tritchler D, Parkhomenko E, Beyene J. Filtering Genes for Cluster and Network Analysis;10(1):193. doi:10.1186/1471-2105-10-193.
60. Carcamo-Orive I, Hoffman GE, Cundiff P, Beckmann ND, D’Souza SL, Knowles JW, et al. Analysis of Transcriptional Variability in a Large Human iPSC Library Reveals Genetic and Non-Genetic Determinants of Heterogeneity;20(4):518–532.e9. doi:10.1016/j.stem.2016.11.005.
61. Maechler M, Rousseeuw P, Struyf A, Hubert M, Hornik K, et al. Cluster: Cluster Analysis Basics and Extensions;1(2):56.
62. Reeves E, James E. Antigen Processing and Immune Regulation in the Response to Tumours;150(1):16–24. doi:10.1111/imm.12675.
63. Hermans MAW, Schrijver B, van Holten-Neelen CCPA, Gerth van Wijk R, van Hagen PM, van Daele PLA, et al. The JAK1/JAK2- Inhibitor Ruxolitinib Inhibits Mast Cell Degranulation and Cytokine Release;48(11):1412–1420. doi:10.1111/cea.13217.
64. Hoadley KA, Yau C, Hinoue T, Wolf DM, Lazar AJ, Drill E, et al. Cell-of-Origin Patterns Dominate the Molecular Classification of 10,000 Tumors from 33 Types of Cancer;173(2):291–304.e6. doi:10.1016/j.cell.2018.03.022.
65. Majzner RG, Heitzeneder S, Mackall CL. Harnessing the Immunotherapy Revolution for the Treatment of Childhood Cancers;31(4):476–485.
66. Cunanan KM, Iasonos A, Shen R, Begg CB, Gönen M. An Efficient Basket Trial Design;36(10):1568–1579. doi:10.1002/sim.7227.
67. Rhee JK, Jung YC, Kim KR, Yoo J, Kim J, Lee YJ, et al. Impact of Tumor Purity on Immune Gene Expression and Clustering Analyses across Multiple Cancer Types;6(1):87–97. doi:10.1158/2326-6066.CIR-17-0201.
68. Raphael BJ, Hruban RH, Aguirre AJ, Moffitt RA, Yeh JJ, Stewart C, et al. Integrated Genomic Characterization of Pancreatic Ductal Adenocarcinoma;32(2):185–203.